Journal of Materials Science and Engineering A 16 (1-3) (2026) 12-25
doi: 10.17265/2161-6213/2026.1-3.002

Numerical Investigation of the h-ETL/$MAPI_{1-x}Cl_x$ Interface for Performance Optimization of Perovskite Solar Cells

Boureima Traore, Valentin Tapsoba, Adama Zongo, Issiaka Sankara, Soumaïla Ouedraogo and François Zougmoré
Département de Physique, Laboratoire de Matériaux et Environnement (LA.M.E)-UFR/SEA, Université Joseph Ki-ZERBO, 03 BP 7021 Ouagadougou 03, Burkina Faso

Abstract: In this study, numerical modeling based on the SCAPS-1D software is employed to analyze the influence of the h-ETL/$MAPI_{1-x}Cl_x$ interface on the performance of perovskite solar cells. The impact of interface defect density, energy band alignment, and transport parameters of the h-ETL is systematically investigated. The results highlight the existence of a critical interface defect density threshold of approximately 10^{13} cm^{-2}, beyond which device performance significantly deteriorates due to increased non-radiative recombination. A slightly positive conduction band offset, ranging from 0 to + 0.2 eV, is identified as an optimal condition that reduces interfacial recombination without hindering electron transport. The study also shows that increasing the electron mobility of the h-ETL has a negligible effect on the overall cell performance. Finally, a combined optimization of absorber and h-ETL doping reveals that moderate acceptor doping of the absorber, coupled with high donor doping of the h-ETL, enhances the internal electric field, limits recombination losses, and improves charge extraction. These findings provide valuable guidelines for the design and optimization of interfaces in high-efficiency perovskite solar cells.

Key words: Perovskite solar cells, $MAPI_{1-x}Cl_x$, h-ETL, interface defects, SCAPS-1D.

1. Introduction

Perovskite solar cells (PSCs) have emerged as one of the most promising photovoltaic technologies, with certified power conversion efficiencies exceeding 26% in just over a decade [1]. This rapid progress is attributed to the exceptional optoelectronic properties of hybrid organic–inorganic perovskites, such as a high absorption coefficient, long charge-carrier diffusion lengths, and a tunable bandgap [2, 3]. Among the various compositions investigated, methylammonium lead iodide chloride ($MAPI_{1-x}Cl_x$) has attracted particular attention due to its improved crystallinity, enhanced carrier mobility, and reduced recombination losses compared to pure $MAPbI_3$ [4, 5]. The incorporation of chlorine promotes grain growth and passivation of bulk and interfacial defects, resulting in improved device performance and stability [6]. Electron transport layer (ETL) materials used in PSCs have enabled high efficiencies; however, they still present several drawbacks, including high processing temperatures and a high density of surface states, which may limit device performance and long-term stability [7, 8]. In this context, the search for alternative electron transport layers has become a major research focus. Hydride-based layers (h-ETLs) have emerged as promising candidates due to their wide bandgaps, good electron conductivity, low trap-state density, and compatibility with low-temperature fabrication processes [9, 10]. The integration of an h-ETL into $MAPI_{1-x}Cl_x$-based PSCs could provide improved energy band alignment, promote more efficient electron extraction, and reduce interfacial recombination losses [11]. Despite these advances, non-radiative recombination at interfaces

Corresponding author: Boureima Traore, Ph.D., research field: semiconductor physics as applied to solar PV.

remains a major challenge, particularly at the h-ETL/perovskite absorber interface [12]. This interface governs charge extraction, energy band alignment, and defect-assisted recombination, directly influencing the open-circuit voltage and fill factor [13]. Recently, hydride or hybrid electron transport layers (h-ETLs) have been proposed as promising alternatives to conventional ETLs, offering tunable electronic properties and improved interfacial compatibility with perovskites [14, 15]. Understanding and optimizing recombination mechanisms at the h- ETL/MAPI$_{1-x}$Cl$_x$ interface especially those related to band alignment and interface defect density constitute a key challenge for sustainably improving PSC performance. Recent studies have shown that the conduction band offset (CBO) at the h-ETL/MAPI$_{1-x}$Cl$_x$ interface directly affects electron transport and interfacial recombination. A slightly positive CBO can act as a selective barrier that suppresses recombination while maintaining efficient electron transport [16, 17].

Similarly, controlling doping levels and the internal electric field represents an important strategy for enhancing charge separation and improving overall device performance [18]. In this context, numerical simulation tools such as SCAPS-1D provide effective means to analyze dominant physical mechanisms and optimize device parameters prior to experimental implementation [19]. SCAPS-1D enables systematic investigation of both bulk and interfacial parameters and offers deeper insight into recombination mechanisms [20]. In this work, we present a comprehensive numerical study of the h-ETL/MAPI$_{1-x}$Cl$_x$ interface using SCAPS-1D to identify the key physical parameters governing the performance of perovskite solar cells. The influence of interface defect density, energy band alignment, electron mobility, and the doping levels of both the absorber and the h-ETL is systematically analyzed. The objective is to determine optimal conditions that minimize non-radiative recombination, enhance charge extraction, and provide reliable guidelines for the design of high-efficiency perovskite solar cells.

2. Device Structure and Simulation Methodology

In the field of photovoltaics, researchers use several software tools to analyze the performance of thin-film solar cells. Among these tools are AMPS, SILVACO ATLAS [21, 22], COMSOL, wx-AMPS, PC-1D [23], and SCAPS-1D [24]. In this work, we selected the one-dimensional simulation software SCAPS-1D (version 3.3.10), developed at Ghent University in Belgium by Burgelman et al. [25]. This software offers several advantages, including the ability to analyze device structures composed of up to seven different layers and to perform detailed interface analyses of the solar cell [13]. Furthermore, the results obtained using this software are in good agreement with experimental data reported by other research groups. SCAPS-1D is based on the numerical solution of the fundamental semiconductor equations, namely the Poisson equation (Equation (1)), the electron continuity equation (Equation (2)), and the hole continuity equation (Equation (3)).

$$div(-grad\ \psi) = \frac{q}{\varepsilon}[p(x) - n(x) + N_D^+(x) - N_A^-(x)] \quad (1)$$

$$\nabla \mathrm{Jn} = \mathrm{q}[\mathrm{R(x)} - \mathrm{G(x)}] + \mathrm{q}\frac{\partial n}{\partial t} \quad (2)$$

$$\nabla \mathrm{Jp} = \mathrm{q}[\mathrm{G(x)} - \mathrm{R(x)}] + \mathrm{q}\frac{\partial p}{\partial t} \quad (3)$$

Equation (1) describes the phenomena of electrostatic nature, where ψ is the electrostatic potential; n and p are the densities of free electrons and holes, respectively; and $N+(x)$ and $N-(x)$ are the concentrations of ionized donor and acceptor, respectively. Equations (2) and (3) govern the dynamic equilibrium condition in a semiconductor, where *G* is the generation rate; Rn and *Rp* are the recombination rates of electrons and holes, respectively; and *Jn* and *Jp* are the current densities of electrons and holes, respectively; their terms are found in literature. These are three coupled and nonlinear differential equations whose solutions allow the extraction of the electrical parameters of the solar cell.

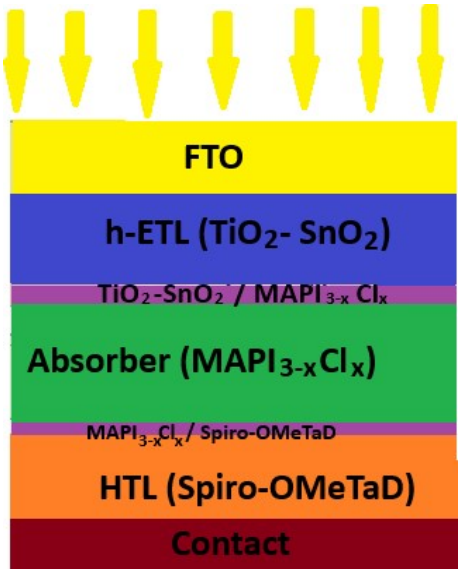

Fig. 1 Modeled structure of a solar cell based on MAPI$_{1-x}$Cl$_x$.

The solar cell investigated in this study is based on a planar n-i-p architecture with the following structure: FTO/h-ETL/MAPI$_{1-x}$Cl$_x$/HTL/Au, as shown in Fig. 1.

In this structure, the glass substrate coated with fluorine-doped tin oxide (FTO) is used as the transparent front electrode, ensuring high optical transmission and good electrical conductivity. The FTO collects the electrons extracted from the hydride electron transport layer (h-ETL). The h-ETL acts as an electron-selective contact, facilitating electron extraction while blocking holes, thereby reducing recombination at the perovskite interface. Its wide bandgap and favorable energy alignment with the conduction band of the perovskite help minimize optical and electrical losses [7, 26]. The h-ETL used in this study is a TiO_2–SnO_2 composite, as it enables a high power conversion efficiency of 20.062%, an open-circuit voltage (V_OC) of 1.179 V, a short- circuit current density (J_SC) of 23.085 mA/cm^2, and a fill factor of 73.671% [27]. These values are in good agreement with those reported for experimental planar perovskite solar cells in benchmark studies [28]. The MAPI$_{1-x}$Cl$_x$ absorber layer is deposited on the h-ETL and constitutes the active region of the solar cell. It is responsible for photon absorption and charge-carrier pair generation. The incorporation of chlorine into the MAPI absorber improves crystallinity and passivates deep defects, which numerically translates into a reduction of Shockley–Read–Hall (SRH) recombination rates. The hole transport layer (HTL), deposited to ensure efficient extraction of photogenerated holes toward the back electrode, is Spiro-OMeTAD (2,2',7,7'- tetrakis(N,N-p-dimethoxyphenylamino)-9,9'-spirobifluorene), due to its favorable energy alignment with the perovskite and its high hole-transport efficiency [29].

The Fig. 2 illustrates the energy band diagram at the h-ETL/MAPI$_{1-x}$Cl$_x$ interface as well as the distribution of the internal electric field. The strong doping difference between the h-ETL (heavily n-type doped) and the absorber (lightly doped) induces band bending near the interface, generating an electric field directed from the absorber toward the h-ETL. The physical parameters of the different layers including bandgap energy, electron affinity, carrier mobility, doping concentrations, and defect densities are selected from experimental data and previously reported numerical studies in the literature [9, 30-36].

The simulations were carried out using an incident power of 1,000 W/m^2, with the perovskite solar cell temperature maintained at 300 K and illuminated under standard AM 1.5 G spectrum conditions, which account for both direct and diffuse radiation. These conditions correspond to international standards for the evaluation of photovoltaic devices [3]. To validate the reliability of our numerical model developed using SCAPS, the simulated photovoltaic parameters were compared with experimental data reported in the literature for MAPI$_{1-x}$Cl$_x$ or MAPI-based perovskite solar cells employing inorganic or hybrid ETLs.

The simulated results are in good agreement with those reported in the literature for MAPI$_{1-x}$Cl$_x$ based perovskite solar cells, confirming the reliability and robustness of the simulation model for PSC optimization prior to fabrication. Any slight discrepancies between simulated and experimental results may be attributed to the absence, in the SCAPS model, of certain extrinsic

losses such as morphological inhomogeneities, contact resistances, and fabrication-related degradation effects [12, 13]. For our PSC structure, the interface defect density was varied over several orders of magnitude in order to identify a critical threshold likely to significantly affect device performance. Furthermore, the conduction band offset (CBO) at the h-ETL/MAPI$_{1-x}$Cl$_x$ interface was adjusted by modifying the electron affinity of the materials to investigate the influence of energy band alignment on recombination and charge extraction [37]. The doping levels of both the absorber and the h-ETL were parameterized to analyze their effect on the internal electric field and carrier separation.

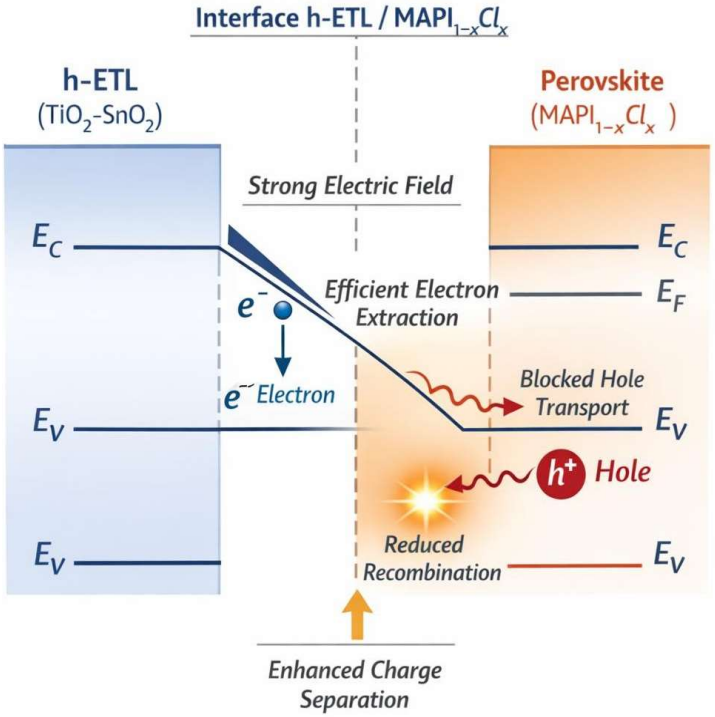

Fig. 2 Energy Band Alignment and Electric Field Distribution at the h-ETL/MAPI$_{1-x}$Cl$_x$ Interface.

Table 1 SCAPS-1D input parameters of the materials used in the simulation.

	FTO	TiO_2–SnO_2	$MAPI_{3-x}Cl_x$	Spiro- OMeTAD
Thickness (nm)	0.27	50	0.333	0.15
Band gap (eV)	3.5	3.3	1.55	3
Electron Affinity (eV)	4.7	4	3.9	2.45
Diélectric relative Permittivity	9	9	6.5	3
Effective density of state in BC (cm^{-3})	$2.2 * 10^{18}$	$2.1 * 10^{18}$	$2.2 * 10^{18}$	10^{19}
Effective density of state in BV (cm^{-3})	$1.8 * 10^{19}$	$1.8 * 10^{19}$	$1.8 * 10^{19}$	10^{19}
Electrons thermal velocity (cm/s)	10^7	10^7	10^7	10^7
Holes thermal velocity (cm/s)	10^7	10^7	10^7	10^7
Electrons Mobility (cm^2/Vs)	33	30	2	10^{-4}
Holes Mobility (cm^2/Vs)	8	15	2	10^{-4}
Donor density N_D (cm^{-3})	10^{18}	2.10^{20}	-	-
Acceptor density N_A (cm^{-3})	-		10^{15}	$2 * 10^{18}$
Bulk defect properties				
Bulk defect Density (cm^{-3})	10^{17}	10^{15}		10^{15}
Capture cross-section electrons (cm^2)	10^{-19}	2.10^{-14}		10^{-14}
Capture cross-section trous (cm^2)	10^{-19}	2.10^{-14}		2.10^{-14}

Table 2 Electrical parameters of the simulation compared with experimental values.

Electrical Parameter	Numérical simulation	Experimental	Références
η (%)	20.062	18-22	[13, 38]
FF (%)	73.671	70-80	[38, 39]
V_{OC} (V)	1.179	1-1.1	[2, 39]
J_{SC} (mA/cm^2)	23.085	22-24	[38, 39]

3. Results and Discussion

3.1 Interface Defect Density at the h-ETL/MAPI$_{1-x}$Cl$_x$ Interface

The interface defect density at the h-ETL/MAPI$_{1-x}$Cl$_x$ junction is a critical parameter that directly influences non-radiative carrier recombination centers and the energy band alignment of perovskite solar cells (PSCs). In the literature, the interface defect density is commonly considered within a range from 10^8 cm^{-2} to 10^{15} cm^{-2}, depending on interface quality and experimental conditions. In this work, the interface defect density at the h-ETL/MAPI$_{1-x}$Cl$_x$ interface was also varied from 10^8 cm^{-2} to 10^{15} cm^{-2}, as shown in Fig. 3.

Fig. 3 illustrates the evolution of the electrical parameters as a function of the interface defect density at the h-ETL/MAPI$_{1-x}$Cl$_x$ interface, denoted as *Nti*. The results show that for low interface defect densities (*Nti* < 10^{13} cm^{-2}), the cell performance remains nearly unchanged. In this range, interfacial recombination remains negligible compared to bulk recombination in the absorber layer, indicating a sufficiently passivated interface and efficient charge transport. In contrast, when the interface defect density exceeds a critical threshold (*Nti* $\geq 10^{13}$ cm^{-2}), a significant degradation of all electrical parameters is observed. The power conversion efficiency drops sharply, reflecting increased Shockley–Read–Hall (SRH) recombination losses induced by trap states at the h-ETL/absorber interface [38, 40]. The open-circuit voltage (V_{OC}) is particularly sensitive to the increase in *Nti*. A high density of trap states introduces deep energy levels within the bandgap, promoting non-radiative recombination and reducing the quasi-Fermi level splitting. The short-circuit current density (J_{sc}) exhibits a more gradual decrease with increasing *Nti*. A high interface defect density enhances interfacial recombination, thereby limiting the efficient collection of photogenerated carriers, particularly electrons extracted through the h-ETL layer.

Similarly, the fill factor (FF) remains high at low defect densities before declining at high *Nti* values. These results highlight the existence of a critical interface defect density threshold beyond which device performance becomes severely limited. They emphasize the crucial role of interface passivation at the h-ETL/MAPI$_{1-x}$Cl$_x$ junction in reducing *Nti* below approximately 10^{13} cm^{-2}, a necessary condition for maintaining a high V_{OC}, an optimal fill factor, and maximum power conversion efficiency. The introduction of an ultra-thin interfacial layer, typically on the order of a few nanometers, can be employed as an effective strategy to reduce the interface defect density by passivating dangling bonds and structural defects responsible for Shockley–Read–Hall recombination [41].

3.2 Energy Band Alignment at the h-ETL/MAPI$_{1-x}$Cl$_x$ Interface

In perovskite solar cells, the energy band alignment at the interface between the h-ETL and the MAPI$_{1-x}$Cl$_x$ absorber is crucial for carrier transport and the reduction of non-radiative recombination. This alignment is commonly quantified by the conduction band offset (CBO), defined as the energy difference between the conduction band minimum of the absorber and that of the h-ETL. Band alignment can be tuned by modifying the electron affinity of the h-ETL. The analytical expression for the conduction band offset is given by:

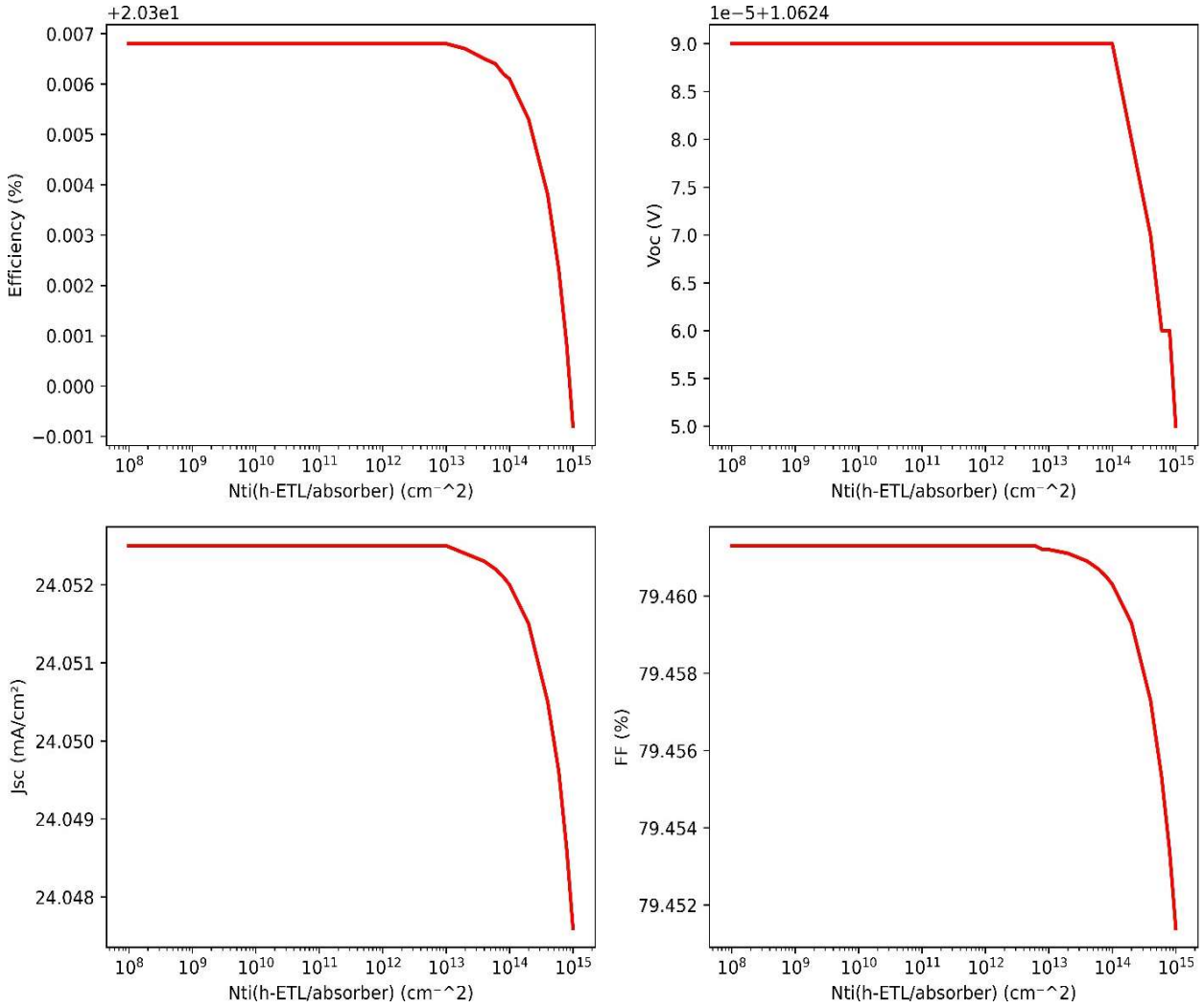

Fig. 3 Influence of Interface Defect Density on the Electrical Parameters.

Table 3 Conduction band offset (CBO) and band alignment values at the h-ETL/perovskite interface.

Perovskite/h-ETL	Electron affinity of Perovskites (eV)	Electron affinity of hybrid h-ETL (eV)	CBO (eV)	Band alignment
MAPI$_{1-x}$Cl$_x$ / TiO$_2$-SnO$_2$	3.9	4	-0.1	Shape Cliff

$$CBO = (X_{abs} - X_{h\text{-}ETL})$$

According to the above equation, the values of the conduction band offset between the absorber and the h-ETL were calculated, and the obtained results are presented in Table 3.

Table 3 shows that the conduction band offset is negative (CBO = –0.1 eV) at the MAPI$_{1-x}$Cl$_x$/TiO$_2$-SnO$_2$ interface. This means that the conduction band minimum of the h-ETL lies below that of the perovskite absorber. Such a value results in a cliff-type band alignment, as illustrated in Fig. 4.

Although this configuration does not introduce any barrier to electron extraction, it strongly promotes carrier recombination at the interface, leading to a reduction in the open-circuit voltage and fill factor. Consequently, the overall efficiency of the PSC is penalized, despite a relatively unchanged short-circuit current density. These results emphasize the importance of tuning the electron affinity of the h-ETL to achieve a slightly positive CBO for optimal device performance. In the following section, we investigate the influence of the conduction band offset

(CBO) at the h-ETL/MAPI$_{1-x}$Cl$_x$ interface by varying it from –0.5 eV to +0.5 eV. This variation is achieved by keeping the electron affinity of the absorber constant while adjusting that of the h-ETL from 4.4 eV to 3.4 eV.

Fig. 5 presents the evolution of the electrical parameters as a function of the conduction band offset (CBO) at the h-ETL/MAPI$_{1-x}$Cl$_x$ interface. The results show that the CBO at the h- ETL/MAPI$_{1-x}$Cl$_x$ interface plays a decisive role in optimizing the performance of the perovskite solar cell. When the CBO is negative (cliff configuration), a marked degradation in efficiency is observed, mainly due to increased interfacial recombination. This enhanced recombination limits the quasi-Fermi level splitting, leading to a significant reduction in the open-circuit voltage (V_{oc}) and fill factor (FF). As the CBO becomes slightly positive, a moderate spike forms at the interface, improving electron selectivity by effectively blocking holes while maintaining efficient electron extraction. This configuration results in a simultaneous increase in V_{oc}, FF, and consequently the overall power conversion efficiency of the device, while the short-circuit current density (J_{SC}) remains nearly unchanged. This indicates that carrier generation and collection within the absorber are not strongly affected by band alignment within this CBO range. A slightly positive CBO, typically between 0 and +0.2 eV, therefore appears to be an optimal compromise between suppressing interfacial recombination and avoiding excessive barriers to electron transport. These findings are in excellent agreement with previous studies based on SCAPS simulations and experimental devices, which report that a moderate spike at the ETL/perovskite interface reduces non-radiative losses and improves the electronic quality of the interface, whereas a cliff configuration enhances interfacial recombination and limits V_{oc} [10, 42]. Studies published in Solar Energy Materials & Solar Cells also confirm that CBO optimization is a key lever for maximizing the performance of planar perovskite solar cells, while reports in Applied Physics Letters highlight the particular sensitivity of V_{oc} and FF to conduction band alignment at the ETL/absorber interface [43].

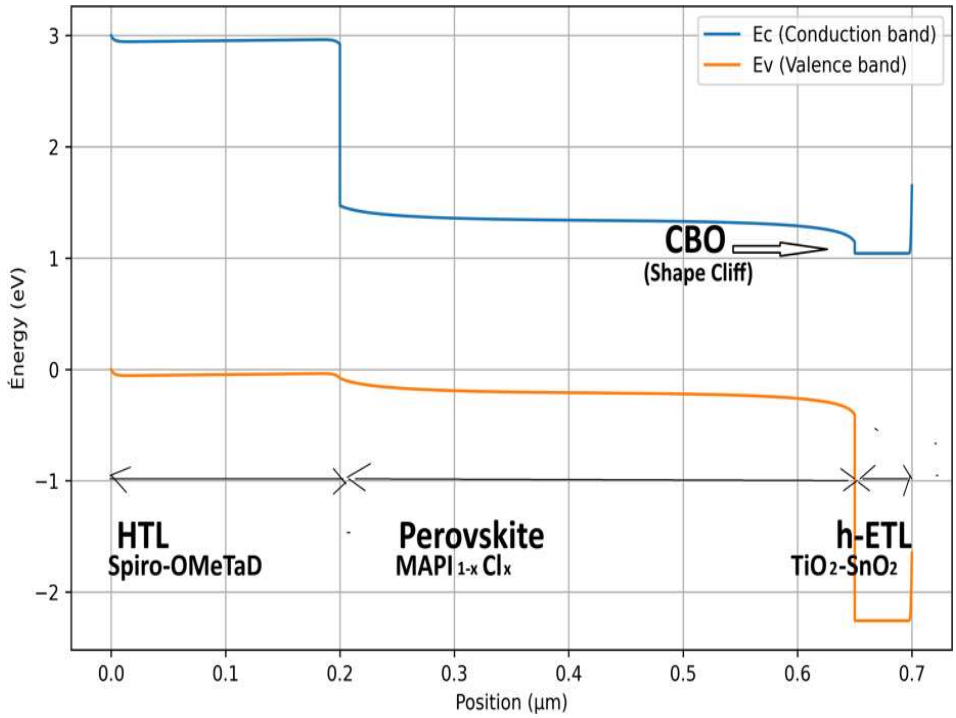

Fig. 4 Energy band diagram of the PSC highlighting the CBO.

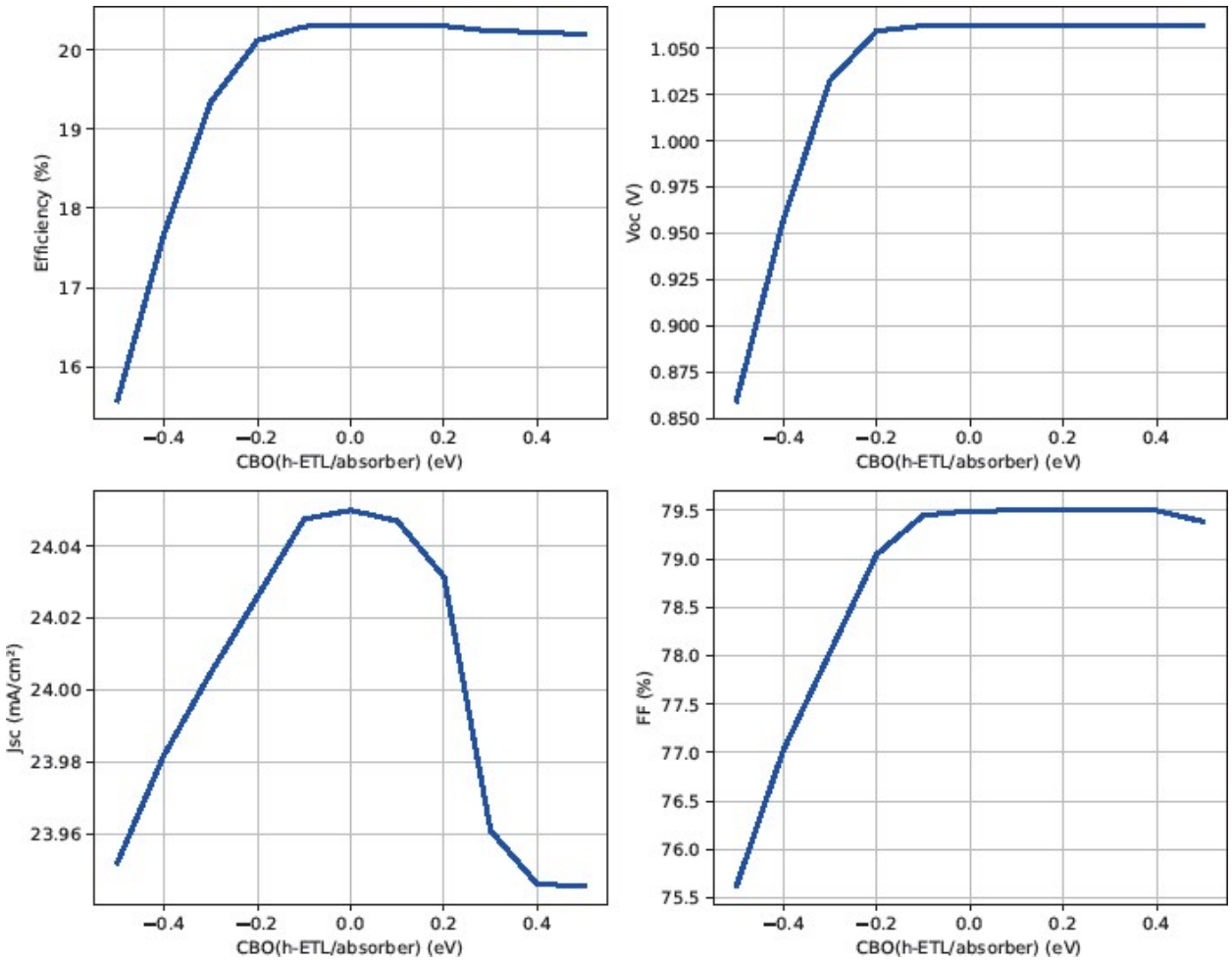

Fig. 5 Influence of Conduction Band Offset (CBO) on the Electrical Parameters.

3.4 Influence of h-ETL Electron Mobility on Electron Extraction at the MAPI$_{1-x}$Cl$_x$/h-ETL Interface

Efficient extraction of photogenerated electrons at the interface between the MAPI$_{1-x}$Cl$_x$ absorber layer and the hybrid electron transport layer (h-ETL) is a key factor determining the performance of perovskite solar cells. In addition to energy band alignment and interface defect density, the electron mobility of the h-ETL (μ_n) plays an important role in charge transport and in limiting interfacial recombination losses. In this study, the electron mobility of the h-ETL was systematically varied from 10^{-2} to 10^{2} cm^2 v^{-1} s^{-1}, while keeping all other device parameters constant, in order to investigate its influence on the electrical performance of the cell. Fig. 2 shows the effect of h-ETL electron mobility on the power conversion efficiency and open-circuit voltage. The curve reveals only a slight variation in efficiency (η) as the electron mobility of the h-ETL increases from 10^{-2} to approximately 2 × 10 cm^2 v^{-1} s^{-1}. Beyond 2 × 10 cm^2 v^{-1} s^{-1}, the efficiency remains nearly constant. This weak dependence indicates that electron mobility is not the main limiting factor for electron transport in the PSC. The dominant losses in PSCs are more likely associated with interfacial recombination or band misalignment at the h-ETL/MAPI$_{1-x}$Cl$_x$ interface. Similar observations have been reported in the literature, where increasing mobility beyond a critical threshold results in only marginal efficiency improvement [13]. Regarding the open-circuit voltage (V_{oc}), it exhibits a maximum for intermediate mobility values between 1 and 10 cm^2 v^{-1} s^{-1}, followed by a slight decrease at higher mobilities.

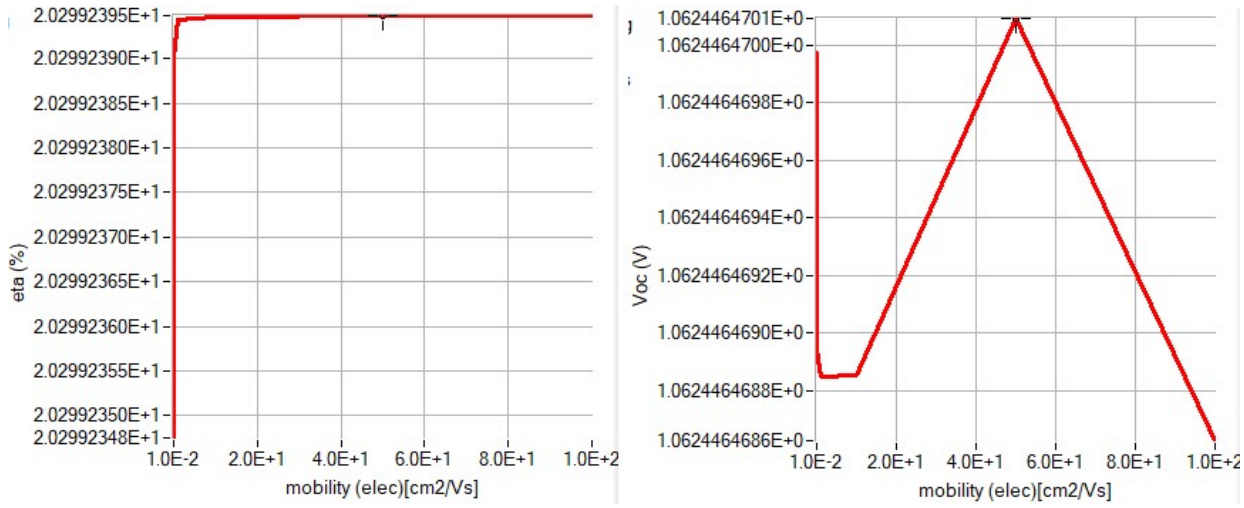

Fig. 6 Influence of h-ETL Electron Mobility on the Electrical Parameters (V_{oc}, η).

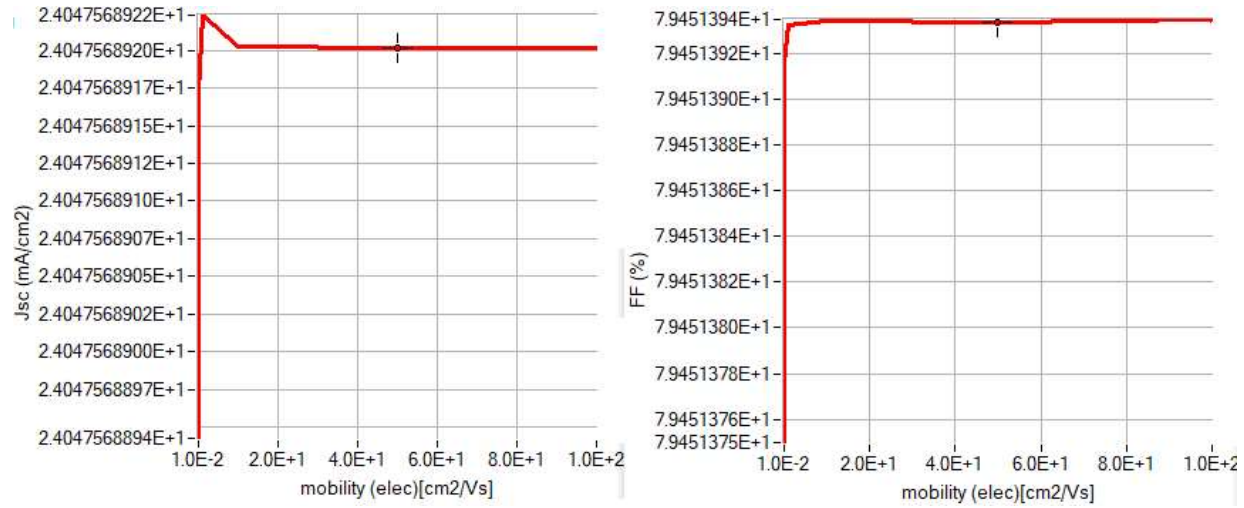

Fig. 7 Influence of h-ETL Electron Mobility on the Electrical Parameters (J_{sc}, FF).

The short-circuit current density (J) and the fill factor (FF) increase rapidly at low mobility values, then reach a saturation regime for mobilities higher than approximately 10 cm^2 v^{-1} s^{-1}. This behavior indicates that the collection of photogenerated carriers becomes nearly optimal, and that J_{SC} is primarily governed by interface quality rather than by the electron mobility of the h-ETL [38]. These results show that the electron mobility of the h-ETL mainly influences V_{oc}, while FF, J_{SC}, and the overall efficiency remain weakly sensitive beyond a threshold value. This confirms that performance optimization of the cell relies more on reducing interfacial recombination and improving energy band alignment at the h-ETL/MAPI$_{1-x}$Cl$_x$ interface than on excessively increasing electron mobility.

3.5 Combined Influence of h-ETL and Absorber Doping

The doping of functional layers plays a crucial role in modulating the internal electric field within the space-charge region (SCR) and, consequently, in determining the performance of perovskite solar cells. In particular, the simultaneous optimization of the doping levels of the h-ETL and the MAPI$_{1-x}$Cl$_x$ absorber enables control over the electrostatic potential distribution and the width of the SCR at the h-ETL/absorber interface. In the literature, donor doping of the h-ETL typically ranges from 10^{16} to 10^{19} cm^{-3} to

ensure sufficient electron conductivity and to enhance band bending near the interface [2, 3]. A high h-ETL doping level promotes the formation of a strong electric field directed toward the h-ETL, facilitating the extraction of photogenerated electrons and reducing their accumulation at the interface. This results in an increase in the fill factor (FF) and open-circuit voltage (V_{oc}) [2, 44]. In contrast, the doping level of the perovskite absorber should remain moderate. Experimental and numerical studies report donor or acceptor concentrations ranging from 10^{13} to 10^{16} cm^{-3} for hybrid perovskites such as MAPI or MAPI$_{1-x}$Cl$_x$ [4, 5, 12]. A lightly doped absorber allows the depletion region to extend deeper into the perovskite layer, thereby maximizing the internal electric field and promoting drift-dominated charge transport rather than diffusion. Conversely, excessive absorber doping leads to electric field screening, a reduction in the space-charge region width, and increased non-radiative recombination, resulting in a simultaneous degradation of V_{oc} and power conversion efficiency (η) [45]. Therefore, the optimal combination consists of a highly doped h-ETL ($\approx 10^{18}$ cm^{-3}) coupled with a lightly doped absorber ($\approx$ 10^{14}-10^{15} cm^{-3}). This configuration maximizes the interfacial electric field, minimizes recombination at the h-ETL/MAPI$_{1-x}$Cl$_x$ interface, and leads to superior photovoltaic performance, as confirmed by SCAPS simulations and consistent experimental findings [3, 12, 44].

Fig. 8 presents the evolution of the electrical parameters of the perovskite solar cell as a function of the acceptor doping (N_a) of the absorber and the donor doping (N_D) of the h-ETL layer. The variations in open-circuit voltage (V_{oc}), short-circuit current density (J_{SC}),

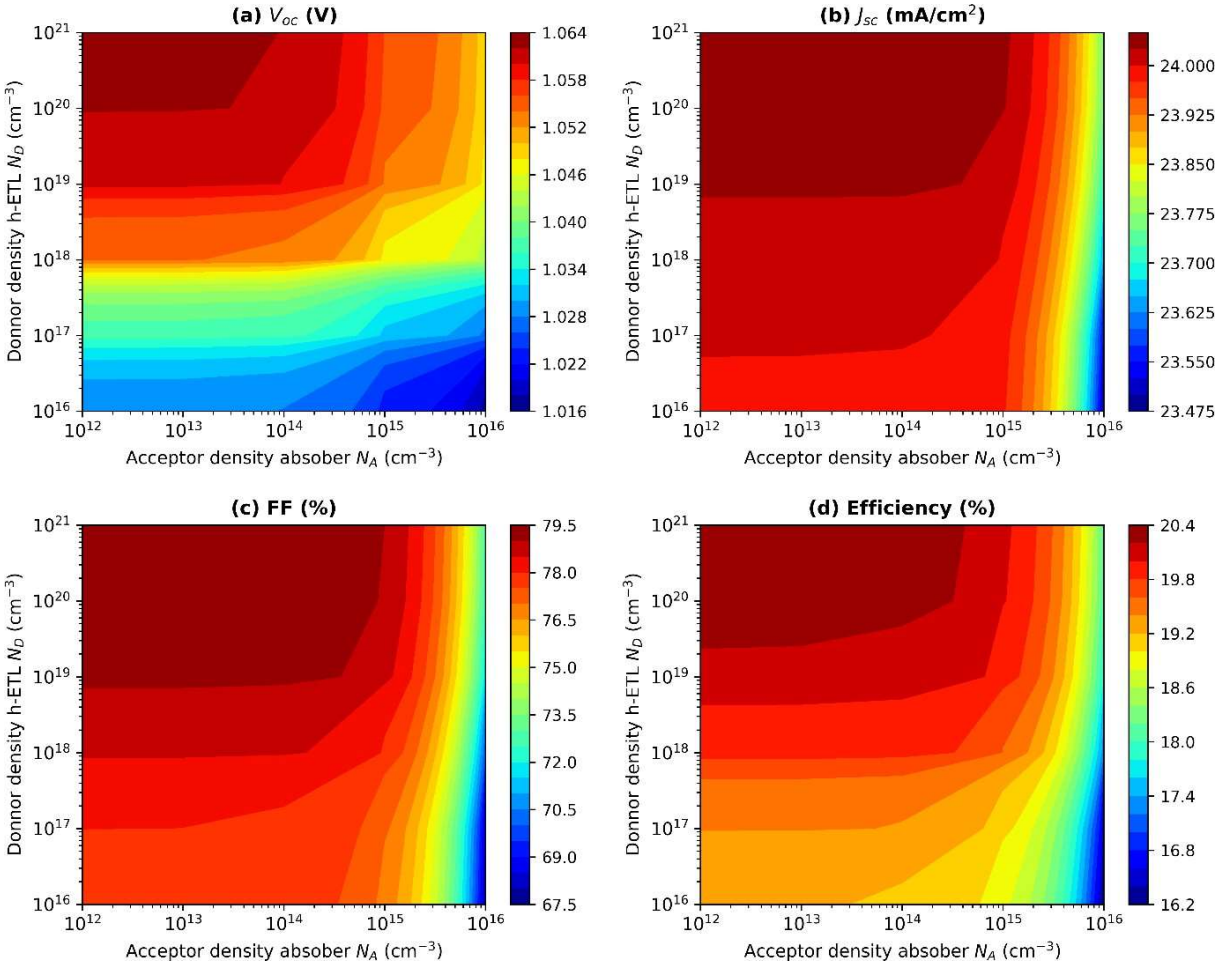

Fig. 8 Influence of h-ETL Doping as a Function of Absorber Doping on the Electrical Parameters.

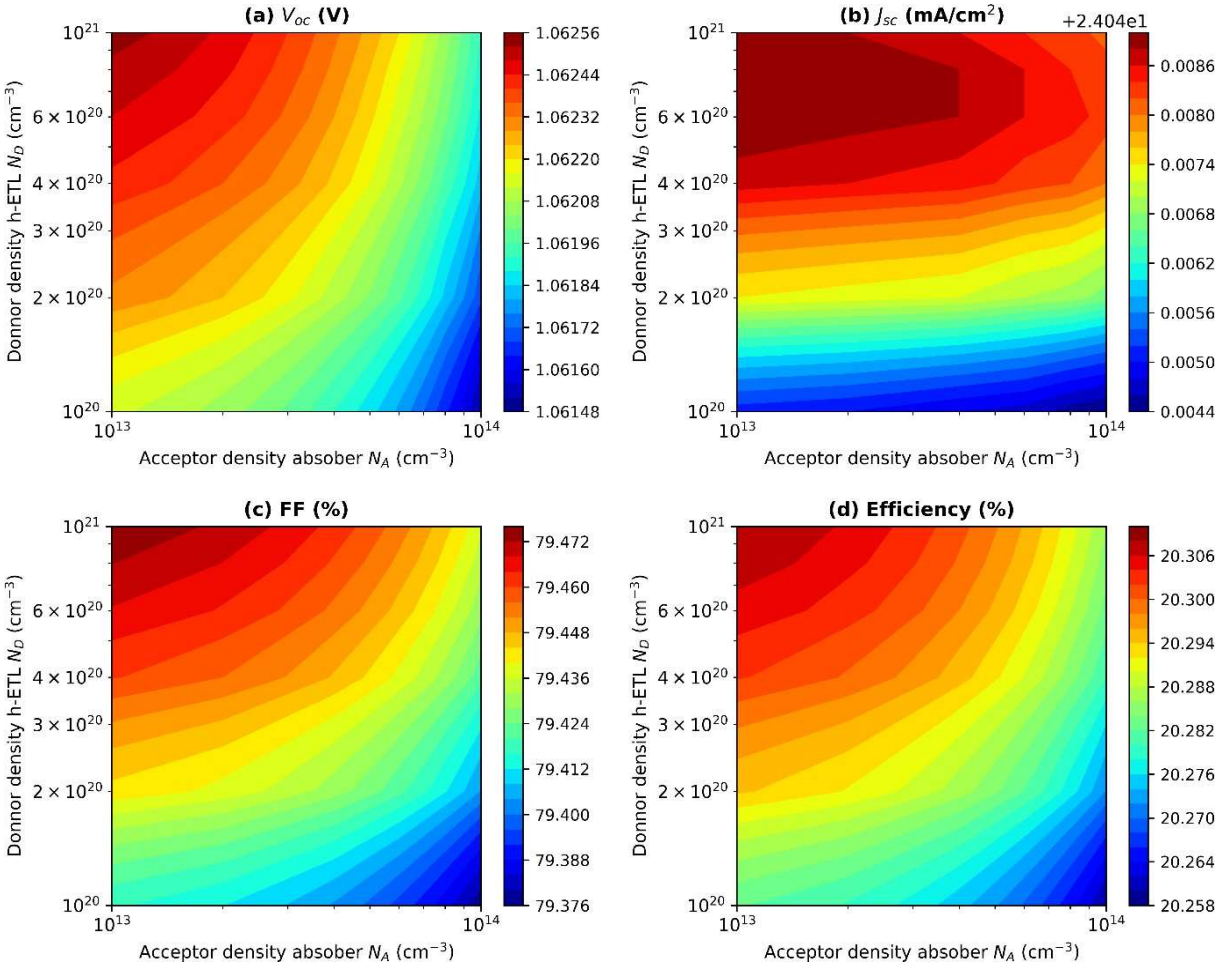

Fig. 9 Influence of h-ETL Doping as a Function of Absorber Doping on the Electrical Parameters.

fill factor (FF), and efficiency (η) highlight the strong dependence of PSC performance on both the donor doping of the h-ETL and the acceptor doping of the MAPI$_{1-x}$Cl$_x$ absorber. In general, all electrical parameters improve with increasing h-ETL doping, while they decrease with increasing absorber doping. A monotonic increase in V_{oc} is observed as the h-ETL doping level increases, particularly for $N_D \geq 10^{18}$ cm^{-3}. In contrast, for high acceptor doping levels ($N_a > 10^{15}$ cm^{-3}), a slight degradation of V_{oc} is observed, as shown in Fig. 8a.

The short-circuit current density (J_{SC}) remains nearly constant for low acceptor doping levels ($N_a \leq 10^{14}$ cm^{-3}), indicating efficient collection of photogenerated carriers within the absorber. However, for higher values ($N_a \geq 10^{15}$ cm^{-3}), a gradual decrease in J_{SC} appears, particularly when the donor density (N_D) is also high (Fig. 8b). This reduction can be attributed to a decrease in carrier diffusion length and enhanced bulk recombination within the absorber. These observations are consistent with analytical and numerical PSC models reported in the literature [41, 46]. The fill factor shows significant improvement with increasing N_D, reaching values above 78-79% for $N_D \geq 10^{19}$ cm^{-3}. Conversely, excessive acceptor doping of the absorber ($N_a \geq 10^{15}$ cm^{-3}) leads to FF degradation, associated with increased resistive and recombination losses [13]. Regarding the power conversion efficiency, very high efficiencies are obtained for absorber doping levels between 10^{13} and 10^{14} cm^{-3} and h-ETL doping levels between 10^{19} and 10^{20} cm^{-3}. In this region, the maximum efficiency ranges from 20% to 20.4%, corresponding to an optimal internal electric field, minimal recombination, and nearly ideal charge

extraction. For excessively high acceptor doping, even though V_{oc} may remain relatively high, the reduction in J_{SC} and FF leads to an overall degradation in efficiency η [44]. This study highlights the existence of an optimal doping window for maximizing perovskite solar cell performance. A moderately doped absorber combined with a highly doped h-ETL promotes a strong internal electric field, limits recombination losses, and results in conversion efficiencies exceeding 20%. To precisely determine the optimal donor and acceptor densities for PSC optimization, a cross-analysis of absorber doping (N_a) and h-ETL doping (N_D) will be performed within the ranges 10^{13} cm^{-3} ≤ N_a ≤ 10^{14} cm^{-3} and 10^{20} cm^{-3} ≤ N_D ≤ 10^{21} cm^{-3}, as illustrated in the figure

It is observed that increasing N_D from 10^{20} to (6-8) × 10^{20} cm^{-3} leads to a significant improvement in V_{oc}, FF, J_{sc}, and η. This trend is attributed to the strengthening of the electric field at the h-ETL/absorber interface, which promotes selective electron extraction and reduces interfacial recombination [47]. For N_D values approaching 10^{21} cm^{-3}, the electrical parameters tend to saturate, indicating that excessive doping no longer provides significant performance gains, in agreement with results reported in the literature [48]. At low acceptor density (N_a ≈ 10^{13} cm^{-3}), the electrical parameters reach their maximum values. Moderate doping limits bulk recombination in the absorber and improves carrier diffusion length [46]. In contrast, increasing N_a toward 10^{14} cm^{-3} results in a gradual degradation of performance, mainly due to the increase in recombination centers and the weakening of the internal electric field [49]. Optimal performance is achieved for N_D = 5 × 10^{20} cm^{-3} and N_a = 2 × 10^{13} cm^{-3}, leading to a maximum efficiency of approximately 20.40%. This combination ensures favorable interfacial band alignment, efficient carrier separation, and reduced recombination losses, in excellent agreement with previous numerical and experimental studies on PSCs optimized through doping engineering [50]. These results confirm that the simultaneous optimization of high donor doping in the h-ETL and moderate acceptor doping in the absorber is a key strategy for controlling the interfacial electric field, leading to significant improvement in the overall performance of perovskite solar cells.

4. Conclusion

This numerical study based on SCAPS-1D highlights the decisive role of the h-ETL/MAPI$_{1-x}$Cl$_x$ interface in determining the performance of perovskite solar cells. Interface defect density, energy band alignment, electron mobility, and the doping levels of the layers surrounding the h- ETL/MAPI$_{1-x}$Cl$_x$ interface are identified as key parameters governing non-radiative recombination. The results reveal the existence of a critical interface defect density threshold on the order of 10^{13} cm^{-3}, beyond which cell performance becomes severely limited. Regarding the conduction band offset, a slightly positive CBO, ranging between 0 and + 0.2 eV, appears to be an optimal compromise between suppressing interfacial recombination and avoiding excessive barriers to electron transport. The study of h-ETL electron mobility shows that even a substantial increase in mobility has almost no significant impact on PSC performance. Finally, a combined investigation of absorber and h-ETL doping demonstrates that moderate acceptor doping of the absorber together with high donor doping of the h-ETL optimizes the internal electric field, reduces recombination losses, and enhances charge extraction. The obtained results provide clear guidelines for the design and experimental development of high-efficiency perovskite solar cells.

References

[1] Energy, N. T. 2024. *Best Research-Cell Efficiency Chart. URL: https://www. nrel. gov/pv/cellefficiency.*

[2] Kojima, A., Teshima, K., Shirai, Y., and Miyasaka, T. 2009. "Organometal Halide Perovskites as Visible-Light Sensitizers for Photovoltaic Cells." *J. Am. Chem. Soc.* 131 (17): 6050-51.

[3] Green, M. A., Ho-Baillie, A., and Snaith, H. J. 2014. "The Emergence of Perovskite Solar Cells." *Nature Photonics* 8 (7): 506-14.

[4] Mosconi, E., Amat, A., Nazeeruddin, M. K., Gratzel, M.,

and De Angelis, F. 2013. "First-principles Modeling of Mixed Halide Organometal Perovskites for Photovoltaic Applications." *The Journal of Physical Chemistry C* 117 (27): 13902-13.

[5] Zhao, Y., and Zhu, K. 2013. "Charge Transport and Recombination in Perovskite (CH_3NH_3) PbI_3 Sensitized TiO_2 Solar Cells." *The Journal of Physical Chemistry Letters* 4 (17): 2880-4.

[6] Zhao, D., *et al.* 2018. "Efficient Two-Terminal All-Perovskite Tandem Solar Cells Enabled by High-Quality Low-Bandgap Absorber Layers." *Nature Energy* 3 (12): 1093-100.

[7] Leijtens, T., Eperon, G. E., Noel, N. K., Habisreutinger, S. N., Petrozza, A., and Snaith, H. J. 2015. "Stability of Metal Halide Perovskite Solar Cells." *Advanced Energy Materials* 5 (20): 1500963.

[8] Yang, G., Tao, H., Qin, P., Ke, W., and Fang, G. 2016. "Recent Progress in Electron Transport Layers for Efficient Perovskite Solar Cells." *Journal of Materials Chemistry A* 4 (11): 3970-90.

[9] Li, X. *et al.* 2016. "A Vacuum Flash–Assisted Solution Process for High-Efficiency Large-Area Perovskite Solar Cells." *Science* 353 (6294): 58-62.

[10] Zhang, Y., Yu, B., Sun, Y., Zhang, J., Su, Z., and Yu, H. 2024. "An MBene Modulating the Buried SnO_2/Perovskite Interface in Perovskite Solar Cells." *Angewandte Chemie* 136 (27): e202404385.

[11] Bush, K. A. *et al.* 2017. "23.6%-Efficient Monolithic Perovskite/Silicon Tandem Solar Cells with Improved Stability." *Nature Energy* 2 (4): 1-7.

[12] Stolterfoht, M. *et al.*, 2019. "The Impact of Energy Alignment and Interfacial Recombination on the Internal and External Open-Circuit Voltage of Perovskite Solar Cells." *Energy & Environmental Science* 12 (9): 2778-88.

[13] Minemoto T., and Murata, M. 2015. "Theoretical Analysis on Effect of Band Offsets in Perovskite Solar Cells." *Solar Energy Materials and Solar Cells* 133: 8-14.

[14] Wang, Q., Phung, N., Di Girolamo, D., Vivo, P., and Abate, A. 2019. "Enhancement in Lifespan of Halide Perovskite Solar Cells." *Energy & Environmental Science* 12 (3): 865-86.

[15] Subudhi, P., and Punetha, D. 2023. "Pivotal Avenue for Hybrid Electron Transport Layer-Based Perovskite Solar Cells with Improved Efficiency." *Scientific Reports* 13 (1): 19485.

[16] Chen W. *et al.* 2015. "Efficient and Stable Large-Area Perovskite Solar Cells with Inorganic Charge Extraction Layers." *Science* 350 (6263): 944-8.

[17] Liu, D., and Kelly, T. L. 2014. "Perovskite Solar Cells with a Planar Heterojunction Structure Prepared Using Room-Temperature Solution Processing Techniques." *Nature Photonics* 8 (2): 133-8.

[18] Ng, K. K., and Sze, S. M. 2007. *Physics of Semiconductor Devices*. Wiley-Interscience Hoboken, NJ.

[19] Burgelman, M., Decock, K., Khelifi, S., and Abass, A. 2013. "Advanced Electrical Simulation of Thin Film Solar Cells." *Thin Solid Films* 535: 296-301.

[20] Burgelman, M., Nollet, P., and Degrave, S. 2000. "Modelling Polycrystalline Semiconductor Solar Cells." *Thin Solid Films* 361: 527-32.

[21] Hima, A., Lakhdar, N., Benhaoua, B., Saadoune, A., Kemerchou, I., and Rogti, F. 2019. "An Optimized Perovskite Solar Cell Designs for High Conversion Efficiency." *Superlattices and Microstructures* 129: 240-6.

[22] Hamri, Y. *et al.* 2019. "Improved efficiency of Cu (In, Ga) Se_2 Thin Film Solar Cells Using a Buffer Layer Alternative to CdS." *Solar Energy* 178: 150-6.

[23] Singh, B., and Gupta, V. 2022. "Modelling and Simulation of Silicon Solar Cells Using PC1D." *Materials Today: Proceedings* 54: 810-3.

[24] Burgelman, M., Verschraegen, J., Minnaert, B., and Marlein, J. 2007. "Numerical Simulation of Thin Film Solar Cells: Practical Exercises with SCAPS." In *Proceedings* of NUMOS (Int. Workshop on Numerical Modelling of Thin Film Solar Cells, Gent (B), Gent. 2007, UGent & Academia Press.

[25] Burgelman, M., Decock, K., Niemegeers, A., Verschraegen, J., and Degrave, S. 2016. *SCAPS manual.* Ghent, Belgium: University of Ghent.

[26] Kim, H.-S. *et al.* 2013. "Mechanism of Carrier Accumulation in Perovskite Thin-Absorber Solar Cells." *Nature Communications* 4 (1): 2242.

[27] Traore, B., Tapsoba, V., Zongo, A., Soumaila, O., Sankara, I., and Francois, Z. 2026. "Numerical Investigation of Performance in $MAPI_{1-x}Cl_x$ Perovskite Solar Cells Employing Hybrid Electron Transport Layers." *Advances in Materials Physics and Chemistry* 16 (2): 69-85.

[28] Green, M. A., Ho-Baillie, A., and Snaith, H. J. 2014. "The Emergence of Perovskite Solar Cells." *Nature Photon* 8 (7): 506-14.

[29] You, J., *et al.* 2014. "Low-temperature Solution-processed Perovskite Solar Cells with High Efficiency and Flexibility." *ACS Nano*. 8 (2):1674-80.

[30] Patil, P., Mann, D. S., Nakate, U. T., Hahn, Y.-B., Kwon, S.-N., and Na, S.-I. 2020. "Hybrid Interfacial ETL Engineering Using PCBM-SnS2 for High-Performance Pin Structured Planar Perovskite Solar Cells." *Chemical Engineering Journal* 397: 125504.

[31] Targhi, F. F., Jalili, Y. S., and Kanjouri, F. 2018. "$MAPbI_3$ and $FAPbI_3$ Perovskites as Solar Cells: Case Study on Structural, Electrical and Optical Properties." *Results in Physics* 10: 616-27.

[32] Ngue, P. G. D. K., Ngoupo, A. T., Abena, A. M. N., Abega, F. X. A., and Ndjaka, J.-M. B. 2024. "Investigation of the

Performance of a Sb_2S_3-Based Solar Cell with a Hybrid Electron Transport Layer (h-ETL): A Simulation Approach Using SCAPS-1D Software." *International Journal of Photoenergy* 2024: 1-23.

[33] Hossain, M. K., *et al.* 2023. "An Extensive Study on Multiple ETL and HTL Layers to Design and Simulation of High-performance Lead-free $CsSnCl_3$-based Perovskite Solar Cells." *Scientific Reports* 13 (1): 2521.

[34] Sharma, H., Verma, V. K., Singh, R. C., Singh, P. K., and Basak, A. 2023. "Numerical Analysis of High- Efficiency CH3NH3PbI3 Perovskite Solar Cell with PEDOT: PSS Hole Transport Material Using SCAPS 1D Simulator: H. Sharma et al." *Journal of Electronic Materials* 52 (7): 4338-50.

[35] Malla Hasan, H., and Onay, Ö. 2022. "Investigation of the Effect of Different Factors on the Performance of Several Perovskite Solar Cells: a Simulation Study by SCAPS." *European Journal of Engineering Science and Technology*, 5 (1): 20-38.

[36] Kanoun, M. B., Kanoun, A.-A., Merad, A. E., and Goumri-Said, S. 2021. "Device Design Optimization with Interface Engineering for Highly Efficient Mixed Cations and Halides Perovskite Solar Cells." *Results in Physics* 20: 103707,

[37] Anderson, R. 1960. "Germanium-gallium Arsenide Heterojunctions." *IBM Journal of Research and Development* 4 (3): 283-7.

[38] Correa-Baena, J.-P., *et al.* 2017. "Promises and Challenges of Perovskite Solar Cells." *Science* 358 (6364): 739-44.

[39] Saliba, M., Stolterfoht, M., Wolff, C. M., Neher, D., and Abate, A. 2018. "Measuring Aging Stability of Perovskite Solar Cells." *Joule* 2 (6): 1019-24.

[40] Pockett, A. 2016. "Characterization of Perovskite Solar Cells." Doctoral thesis, The University of Bath.

[41] De Wolf, S., *et al.* 2014. "Organometallic Halide Perovskites: Sharp Optical Absorption Edge and its Relation to Photovoltaic Performance." *The Journal of Physical Chemistry Letters* 5 (6):1035-9.

[42] Jiang, Q., *et al.* 2016. "Enhanced Electron Extraction Using SnO_2 for High-Efficiency Planar-Structure HC $(NH_2)_2PbI_3$-based Perovskite Solar Cells." *Nature Energy* 2 (1): 1-7.

[43] Tress, W., Marinova, N., Moehl, T., Zakeeruddin, S. M., Nazeeruddin, M. K., and Grätzel, M. 2015. "Understanding the Rate-dependent J–V Hysteresis, Slow Time Component, and Aging in $CH_3NH_3PbI_3$ Perovskite Solar Cells: the Role of a Compensated Electric Field." *Energy & Environmental Science* 8 (3): 995-1004.

[44] Stranks, S. D., *et al.* 2013. "Electron-hole Diffusion Lengths Exceeding 1 Micrometer in an Organometal Trihalide Perovskite Absorber." *Science* 342 (6156): 341-4.

[45] Subudhi, P., and Punetha, D. 2023. "Pivotal Avenue for Hybrid Electron Transport Layer-based Perovskite Solar Cells with Improved Efficiency." *Sci. Rep.* 13 (1):19485.

[46] Tress, W. 2017. "Metal Halide Perovskites as Mixed Electronic–Ionic Conductors: Challenges and Opportunities from Hysteresis to Memristivity." *The Journal of Physical Chemistry Letters* 8 (13): 3106-14.

[47] Abdelaziz, S., Zekry, A., Shaker, A., and Abouelatta, M. 2022. "Investigation of Lead-free $MASnI_3$-$MASnIBr_2$ Tandem Solar Cell: Numerical Simulation." *Optical Materials*123:111893.

[48] Jeyakumar, R., Bag, A., Nekovei, R., and Radhakrishnan, R. 2020. "Influence of Electron Transport Layer (TiO_2) Thickness and its Doping Density on the Performance of $CH_3NH_3PbI_3$-based Planar Perovskite Solar Cells." *Journal of Electronic Materials* 49 (6): 3533-9.

[49] Du, H.-J., Wang, W.-C., and Zhu, J.-Z. 2016. "Device Simulation of Lead-free $CH_3NH_3SnI_3$ Perovskite Solar Cells with High Efficiency." *Chinese Physics B* 25 (10): 108802.

[50] Islam, M., and Thakur, A. 2020. "Two Stage Modelling of Solar Photovoltaic Cells Based on Sb_2S_3 Absorber with Three Distinct Buffer Combinations." *Solar Energy* 202: 304-15.